HHS Public Access

Author manuscript

Biomater Adv. Author manuscript; available in PMC 2024 September 01.

Published in final edited form as:

Biomater Adv. 2023 December ; 155: 213667. doi:10.1016/j.bioadv.2023.213667.

Hydroxyapatite coated titanium with curcumin and epigallocatechin gallate for orthopedic and dental applications

Priya Kushram,

Ujjayan Majumdar,

Susmita Bose*

W. M. Keck Biomedical Materials Research Laboratory, School of Mechanical and Materials Engineering, Washington State University, Pullman, Washington 99164, United States

Abstract

Titanium and its alloy are clinically used as an implant material for load-bearing applications to treat bone defects. However, the lack of biological interaction between bone tissue and implant and the risk of infection are still critical challenges in clinical orthopedics. In the current work, we have developed a novel approach by first 1) modifying the implant surface using hydroxyapatite (HA) coating to enhance bioactivity and 2) integrating curcumin and epigallocatechin gallate (EGCG) in the coating that would induce chemopreventive and osteogenic potential and impart antibacterial properties to the implant. The study shows that curcumin and EGCG exhibit controlled and sustained release profiles in acidic and physiological environments. Curcumin and EGCG also show *in vitro* cytotoxicity toward osteosarcoma cells after 11 days, and the dual system shows a ~94 % reduction in bacterial growth, indicating their *in vitro* chemopreventive potential and antibacterial efficacy. The release of both curcumin and EGCG was found to be compatible with osteoblast cells and further promotes their growth. It shows a 3-fold enhancement in cellular viability in the dual drug-loaded implant compared to the untreated samples. These findings suggest that multifunctional HA-coated Ti6Al4V implants integrated with curcumin and EGCG could be a promising strategy for osteosarcoma inhibition and osteoblast cell growth while preventing infection.

Keywords

Curcumin; EGCG; Hydroxyapatite; Osteoblast; Osteosarcoma

*Corresponding author. *address:* sbose@wsu.edu (S. Bose).

Declaration of competing interest

The authors declare that they have no known competing financial interests or personal relationships that could have appeared to influence the work reported in this paper.

CRediT authorship contribution statement

Priya Kushram: Methodology, Formal analysis, Conceptualization, Visualization, Writing – original draft, Investigation. **Ujjayan Majumdar:** Methodology, Investigation, Writing – review & editing. **Susmita Bose:** Project administration, Funding acquisition, Supervision, Conceptualization, Validation, Writing – review & editing, Resources.

1. Introduction

The use of synthetic bone grafts to repair bone defects in load-bearing areas is of significant interest in clinical orthopedics. These bone defects occur due to musculoskeletal disorders such as traumatic injuries, osteoporosis, bone infection, and congenital malfunction. [1] Critical-size bone defects do not self-repair and thus require a graft material to repair. [2] As a result, the demand for orthopedic implants has been increasing rapidly. In the US itself, the market for orthopedic implants was $ 46.8 billion in 2018, which is estimated to be around $64 billion by 2026. [3] Globally, the market is estimated to reach $79.5 billion by 2030, which is a 2 fold increase compared to 2019. [4] Osteosarcoma is another bone disease prevalent in children and adolescent patients aged 10 to 30, with a second peak occurring in old age people. [5–7] Since the 1980s, the standard treatment of this malignancy has been with a combination of both limb salvaging surgeries and adjuvant chemotherapy. However, the lack of site-specificity of chemotherapeutic drugs causes toxicity to normal healthy cells. [8] In addition, the current approach does not completely eradicate the tumor cells and also causes large bone defect which is beyond the self-repairing ability of bone. [9] These various challenges fuel the need to fabricate a multifunctional bone substitute that can inhibit osteosarcoma recurrence and eventually heal the bone defect.

Natural medicinal compounds (NMCs) have been gaining significant attention as an alternative strategy to treat osteosarcoma due to their fewer side effects, easy availability, and lower cost. [10] Curcumin (Cur), obtained from the perennial herb *Curcuma longa,* is a widely researched natural medicine known to exhibit antioxidant, anti-inflammatory, and anticancer properties. [11–14] In one of the clinical studies, it was found that oral administration of Cur is easily tolerated up to 12 g/day, indicating that Cur is safe to use. [15] Several preclinical studies have shown that Cur shows anti-cancer properties against many cancer types. [16–18] Additionally, Cur is also found to promote osteogenesis, as demonstrated through an *in vivo* rat distal femur model where Cur treated implant showed better contact with the surrounding bone after 5 days of implantation. [9] Despite its excellent therapeutic activity, limitations such as low solubility and rapid metabolism have reduced its therapeutic efficacy in clinical applications. [19] Recent studies have shown that Cur shows synergistic effects when combined with other drugs. [20]

The combination of Cur with Epigallocatechin Gallate (EGCG), a bioactive constituent from green tea, has inhibited tumor growth in the PDX mouse model with colorectal carcinoma and found that the combined drugs showed a higher anti-angiogenic effect than the individual drug. [21,22] EGCG is known to exhibit anti-inflammatory, anti-oxidative, and anti-cancer properties. [22] It can induce apoptosis in multiple cancer types, including brain, colon, kidney, and lung, through different cell signaling pathways, as studied using both *in vitro* and *in vivo* models. [23,24] EGCG shows anti-cancer effects by modulating the activity of insulin-like growth factor 1 (IGF1) receptor, protein kinase B(Akt), nuclear factor-kappa B (NF- κB), and hypoxia-inducible factor 1α (HIF1α), etc. [25]. Recent studies have also demonstrated the positive effect of EGCG on *in vivo* angiogenesis and osteogenesis. [26,27] Titanium and its alloy, such as Ti6Al4V, have been used as an implant material in high load-bearing sites, in pure and coated form, owing to its excellent biocompatibility, mechanical property and corrosion resistance. [60,61] However, due to

its biological inertness, it does not undergo osseointegration. Instead, it results in fibrous tissue encapsulation and causes implant loosening, therefore hindering its long-term clinical success. [61] Here, the implant's surface is modified with the calcium phosphate coating using plasma spray to improve its bioactivity. [30,31] Hydroxyapatite (HA), a calcium phosphate, is one of the extensively researched bioceramics in bone tissue engineering, owing to its compositional similarity (Ca/P ratio = 1.67) with human bone, resulting in biocompatibility and bioactivity. [35,36]

Implant-related infection is another critical concern in orthopedics surgery, making bone repair challenging in patients. [37] A significant proportion of the infections are caused by multi-drug resistant bacteria, especially *Staphylococcus aureus* (*S. aureus*), accounting for nearly two out of three conditions reported. [38] High doses of synthetic antibiotics to treat these infections cause multi-drug resistance and thus reduce the antibacterial efficacy. Natural medicines such as Cur and EGCG have been known to show antibacterial efficacy against *S. aureus* via different mechanisms. [39,40] The integration of both EGCG and Cur and their local release would also induce antibacterial properties in the implant surface and could prevent local and systemic infection.

Although the effect of individual Cur and EGCG on osteosarcoma and antibacterial properties has been explored, the effect of co-delivery of Cur and EGCG system through HA-coated implant on *in vitro* osteosarcoma inhibition and antibacterial properties has not been studied. This work aims to study the combined effect of co-delivery of EGCG and Cur loaded HA-coated Ti6Al4V implant on *in vitro* osteoblast growth, chemopreventive potential, as well as anti-infection efficacy. We hypothesize that incorporating Cur and EGCG into the HA-coated implant will 1) support and enhance osteoblast cell proliferation and differentiation, 2) inhibit osteosarcoma cell growth, and 3) show antibacterial properties. The novelty of this work is the controlled and sustained co-delivery of Cur and EGCG from HA-coated implants and its effect on biological properties.

2. Materials and methods

2.1. HA-coated Ti6Al4V sample preparation and adhesive strength testing

The HA coating was deposited on a Ti6Al4V disc, cut with dimensions of 12.2 mm diameter and 2 mm thickness, using a water jet from Ti6Al4V plates (Titanium Joe, MA, USA). Before the coating was performed, these cut discs were sandblasted and cleaned in an ultra-sonicator with deionized water. The HA powder (Monsanto, MO, USA) was then sieved to obtain a particle size of <100 μm. Subsequently, the axial coating was performed using a 25 kW RF induction plasma spray system (Tekna Plasma Systems, Canada) with a working distance of 110 mm. [41] Argon gas was used as central and carrier gas with a 25 and 13 standard liters per minute flow rate. The pressure inside the chamber was maintained at 5 psi during the coating operation. The adhesive strength testing was performed based on ASTM C633–13. [42] First, the substrate was mounted on posts using an Armstrong A-12 (Resin Technology Group, LLC, Easton, MA, USA). The testing was carried out in an Instron tensile apparatus (Industrial Series 600 DX Model, Instron, Norwood, MA, USA) with a speed of 13 mm/s until failure. The adhesive strength was calculated by force divided by the surface area of the coating.

2.2. In vitro drug release study at acidic and physiological medium

Individual Cur (≥98.0% Millipore Sigma, St. Louis, USA) and EGCG (97.69 %, APExBIO, USA) solutions were prepared by dissolving them in ethanol at 5 mg/mL and 1 mg/mL, respectively. First, 100 μL of the solution containing 500 μg of Cur was loaded on the coated implant, followed by 100 μL of the solution containing 100 μg EGCG, dissolved in ethanol (100 %, KOPTEC, USA) using the drop-casting method. The release study was investigated at acetate buffer (pH 5.0) and phosphate buffer (pH 7.4). The phosphate buffer was prepared by mixing 13.9 g of potassium phosphate and 2.7 g of monopotassium phosphate in 1 L of deionized water. For acetate buffer, 8.2 g of sodium acetate and 6 g of acetic acid are mixed in 1 L of deionized water. The pH of the buffer media was measured using pH paper. The samples were immersed in the 4 mL buffer solution in a glass vial and placed in the shaker at 150 rpm and 37°C to roughly mimic the human body motion. Three replicates were used for each treatment. The buffer media was collected from the glass vial after 0.5, 1, 2, 4, 6, 8, and 12 h, and then 1, 2, 3, 5, 7, 10, 14, and 21 days to measure the amount of drug released and replaced with 4 mL of fresh buffer media. The amount of drug release was analyzed by obtaining the optical density of collected buffer media using a UV–Vis spectroscopy microplate reader (Biotek Synergy 2 SLEFPTAD, Winooski, VT, USA). The absorbance values for Cur and EGCG were obtained at 427 nm and 278 nm, respectively. Subsequently, the drug concentration was measured with the help of a standard curve and later plotted as the percentage of cumulative release against time. The release kinetics were fit using the Weibull fit and Power law using MATLAB® software. The equations below represent Weibull (1) and Power Law (2).

$$Q(t) = 100 \times \left(1 - exp\left(-\frac{t^a}{b}\right)\right) \quad (1)$$

$$Q(t) = K \times t^n \quad (2)$$

Where $Q(t)$ is the cumulative percentage release at time t, a and b represent the time constant and shape parameter, respectively. [43] The K and n represent the rate constant and release exponent, respectively. [44]

2.3. Surface morphology after release study

The surface morphology of the release study samples was analyzed after 21 days to observe any change in the coating due to different buffers. The samples were first left to dry at 70°C for 24 h. For Scanning Electron Microscopy (SEM) imaging, the samples were first gold coated using a sputter-coater (Jeol, MA, USA) and were then observed under the microscope (FEI, Quanta 200, OR, USA). For the 3D mapping of the implant surface using a stereomicroscope, the samples were left to dry at 70 °C for 24 h. The dried samples were

then observed under the microscope. The 3D mapping of the coated implants was performed under the Keyence microscope (VHX-700, Keyence, USA).

2.4. In vitro cell culture

2.4.1. Osteosarcoma and osteoblast cell culture—All samples before drug loading were sterilized using steam autoclaving at 121°C for 1 h. The MG-63 human osteosarcoma cells (ATCC, USA) were grown in the Eagle's Minimum Essential Media (EMEM, ATCC, USA), with 10 % inactivated fetal bovine serum (ATCC, USA) along with 1 % Penicillin/ Streptomycin (Invitrogen, Germany) in a T-75 flask till they reached ~80–90 % cell confluency. Approximately 25,000 cells were loaded on each sample in a 24-well plate with 1 mL of growth media followed by incubation at 5 % CO_2 and 37°C for culture. The growth media was changed every 2–3 days.

A similar procedure was followed for osteoblast cell culture. The human fetal osteoblast cells (hFOB, 1.19, ATCC, USA) were grown in Dulbecco's Modified Eagle's Media (DMEM, Sigma Aldrich, USA), supplemented with 10 % fetal bovine serum and 1 % Penicillin/Streptomycin in a T-75 cell culture flask till they reached 80–90 % confluency. Approximately 25,000 cells were loaded on each sample in 24 well plates and grown in the incubator at 5 % CO_2 and 37°C.

2.4.2. MTT assay—Cellular viability of osteosarcoma and osteoblast cells was measured using MTT (3-(4,5-dimethylthiazol-2-yl)-2–5-diphenyl tetrazolium bromide) (Sigma, St. Louis, MO, USA) assay. The MTT solution was prepared in PBS at a 5 mg/mL concentration. 100 μL MTT solution and 900 μl of the media were added to samples and incubated for 2 h. 600 μL of the MTT solubilizer was added to samples to dissolve the formazan crystals. MTT solubilizer was prepared using 10 % Triton X-100, 0.1 N HCl, and isopropanol. Subsequently, 100 μL of the solution of each sample was taken to 96-well plates. The optical density of the well plate, having three replicates of each composition, was measured using a microplate reader at 570 nm. Data was presented in the form of mean ± standard deviation. The cell viability percentage of the cells after treatment was calculated using the following equation.

$$Cell\ viability\ (\%) = \frac{Average\ value\ of\ the\ optical\ density\ of\ the\ treatment}{Average\ value\ of\ the\ optical\ density\ of\ the\ control} \times 100$$

2.4.3. ALP assay and immunohistochemistry—After 11 days, samples were washed with 1× ALP assay buffer twice. 20 μL of Triton X-100 is added to 10 mL of 1× assay buffer. 800 μL of this solution is added to the cells. With the help of a scraper, adherent cells are removed, and suspension is collected. The suspensions are then incubated at 4 °C for 10 min and centrifuged at 2500 G for 10 min. 100 μL of this collected supernatant is transferred to 96 well plates. 50 μL of pNPP solution is added to each well, and the well plate is shaken for 1 min in UV–Vis. This is followed by 60 min of incubation period of 25 °C. After this, 50 μL of stop solution is added to each well plate, and optical density at 405 nm is taken. [34]

For ALP staining, the protocol was followed, as reported in our previous work. [45] The samples were first taken from the media, and fixation was done in a 3.7 % paraformaldehyde/PBS at room temperature for 10 min. After washing with PBS, samples were permeabilized with 0.1 % Triton X-100 for 4 min at room temperature. After this, samples were washed with TBST thrice and incubated in TBST-BSA blocking solution for 1 h at room temperature. Next, the primary antibody against ALP at a dilution of 1:100 was added, incubated for 2 h, and then at 4 °C overnight. The samples were then washed with TBST thrice and incubated with a secondary antibody at a dilution of 1:100 in TBST at room temperature for 1 h. After three times washing with TBST, the samples were mounted with DAPI (Invitrogen, US) on the coverslip and kept overnight at 4 °C. The samples were then analyzed using a confocal laser microscope (TCS SP5, Leica, Germany).

2.4.4. Antibacterial study against S. aureus—The antibacterial study was performed against *S. aureus as* per the modified ISO 22196:2011 standard. [46] First, the freeze-dried *S.aureus* bacteria (Carolina Biological Supply Company, Burlington, NC, USA) were rehydrated with 1 mL of rehydrated media. The rehydrated bacteria suspension was transferred to the tube and mixed with the rest of the rehydrating media. Bacteria were incubated for 48 h at 37°C before inoculation. Serial dilution was performed to obtain the bacteria suspension of 1:100. Optical density of the suspension was measured at 625 nm. This was compared with the McFarland standard. The samples were first sterilized using steam autoclaving at 121°C for 1 h. After this, the samples were transferred to a 24-well plate. The 10^6 colony-forming units (CFUs) of bacteria were loaded on the sample for agar plate (Nutrient Agar Plate, Hardy Diagnostic, CA, USA) with 1 mL of Tryptic soy broth media and 10^2 CFUs for SEM. The samples were incubated at 37°C and 90 % humidity and were then analyzed after 36 and 72-h time points using agar plates, live/dead imaging, and SEM. The CFU count was performed from the images of the agar plate and confocal live/dead images with the help of ImageJ (ImageJ software, USA) [8]. The antibacterial efficacy was obtained using the following equation.

$$Antibacterial\ efficacy = \frac{N_{control} - N_{material}}{N_{control}} \times 100 \quad (3)$$

2.4.5. Cell morphology of biological samples—After subsequent time points, the samples were taken out, and 1 mL of 2 % paraformaldehyde/glutaraldehyde in 0.1 M phosphate buffer was added to the samples for cell fixing. The samples were kept overnight at 4°C. Afterward, post-fixation with osmium tetroxide was done for 2 h at room temperature. Next, serial dehydration using ethanol at 30, 50, 70, 90, and 100 % was carried out, followed by HMDS drying. Gold sputter was deposited on the samples before imaging to make them conductive. Finally, surface morphology was evaluated using SEM (FEI, Quanta 200, OR, USA).

2.4.6. Live/dead imaging—Samples after specific time points were taken out and transferred to a different well plate. Equal amounts of propidium iodide (Invitrogen, MA,

USA) and calcein AM (Biolegend, CA, USA) prepared in PBS were added to all samples and incubated for 1 h. Post incubation, imaging *via* confocal microscopy was performed using a confocal microscope (TCS SP5, Leica, Germany). For the detection of calcein, a laser in the range of 485–535 nm was used, while for the detection of propidium iodide, a laser in the range of 530–620 nm was used. Green fluorescence indicates live cells, whereas red indicates dead cells.

2.4.7. Mitochondrial membrane potential assay—After day 7, the samples were transferred to a different 24-well plate and washed with PBS to remove any remaining media. Afterward, they were stained with 2 mM concentrations of JC-1 dye (Invitrogen, MA, USA), followed by incubation for 20 min. Post incubation, the samples were washed with PBS thrice. Fluorescence microscopy was performed using a confocal laser microscope with J-aggregate detected in the 585/590 nm range, showing red fluorescence and JC-1 monomer detected in the range of 510/527 nm, showing green fluorescence.

2.4.8. Statistical analysis—Data from all the experiments are represented as mean ± standard deviation. All statistical analyses were performed using student's *t*-test using GraphPad Prism 8 software. All measurements are representative of three replicates, and p-values ≤ 0.05 are considered significant.

3. Results

3.1. Surface morphology and mechanical characterization of HA-coated Ti6Al4V

The HA coating of the Ti6Al4V implant was performed using RF induction-based plasma spray, having a coating thickness of ~290 μm. Fig. 1A shows the steps involved in fabricating the HA-coated implant and the drug loading step. These drug-loaded implants were then used for the subsequent *in vitro* studies. The micrograph of the HA-coated implant is shown in Fig. 1B. Fig. 1C, D shows the surface morphology of the HA-coated implant with low and high magnification, taken using a stereomicroscope. It shows microroughness across the surface, obtained due to high-temperature plasma coating. Fig. 1E shows the schematic of the pullout test performed to evaluate the adhesive strength of the coating. Loads were applied on both sides and pulled out at a constant rate until the coating came out of the implant. The adhesive strength obtained from the pull-out test came out to be ~17 MPa for untreated HA-coated implant, while Cur and EGCG loaded HA-coated implant showed a strength of ~16 MPa. which aligns with the ASTM-C633–13 standard, according to which the adhesive strength of the coating on the implant should be ≥15 MPa for clinical approval. [47] Fig. 1F, G shows the coating section after the adhesive strength testing with a coating that stays adhered to the implant in Fig. 1F and the section that came out in Fig. 1G.

3.2. Controlled and sustained release of drugs in acidic and physiological environments

The release profiles for each drug after 21 days at pH 5.0 and 7.4 are shown in Fig. 2. At pH 5.0, Cur showed a release of 14.5 %, while at pH 7.4, it became 10 %. The increase in the Cur release % at pH 5.0 than at pH 7.4 could be attributed to the acidic degradation of HA coating, which enhances the release.

The release of Cur in the presence of EGCG (Cur dual) was ~11 % after 21 days, while individual Cur showed 14.5 %. Similarly, at pH 7.4, Cur showed a ~ 10 % release while in the presence of EGCG, it exhibited a ~ 7 % release. The lower release of Cur in the presence of EGCG at pH 5.0 and 7.4 could be because of the hindrance provided by EGCG since EGCG, being in the top layer, partially blocks the interaction of Cur with the surrounding, therefore restricting its release.

At pH 5.0, EGCG showed an initial faster release of ~21 %, followed by sustained release to ~32 % after 21 days. At pH 7.4, EGCG showed a release of 58 % after 21 days. The pKa value of EGCG is 7.68, which is higher than the physiological pH. [48] The higher pKa indicates that there is deprotonation of the acidic phenolic group in the EGCG, leading to higher solubility and, thus, a higher release % in the physiological pH 7.4 compared to pH 5.0.

In the presence of Cur (EGCG dual), EGCG exhibited an increase in the release, which was ~55 % at pH 5.0, while individual EGCG showed ~32 %. A similar pattern was also observed at pH 7.4, where EGCG showed ~58 %, which became ~99 % in the presence of Cur. The release profiles of both EGCG and Cur were fit using power law and weibull fit. [43] Further, SEM images and 3D mapping of before and after release studies shown in Fig. 3 A, B show that higher coating.

3.3. Cur and EGCG show in vitro chemopreventive potential toward bone cancer cells

In vitro cell culture was performed on osteosarcoma cells to evaluate the chemopreventive potential of both EGCG and Cur toward bone cancer cells. Here, an untreated HA-coated implant with no drug was considered as the control. MTT Assay in Fig. 4A shows that cellular viability was reduced for all the compositions at all time points compared to the control. On day 3, a minor difference in cellular viability was observed between the control and different treatments. However, the difference became significant on day 11. On day 11, Cur and EGCG showed ~91 % and ~84 % growth inhibition, which was increased to ~93 % for the dual drug system. Live/dead imaging reveals live osteosarcoma cells in control, as seen through green fluorescence. In contrast, dead osteosarcoma cells were seen in the treated samples, as observed through red fluorescence, shown in Fig. 4B.

Fig. 4C shows the JC-1 assay performed on the osteosarcoma cells to assess the change in mitochondrial membrane potential after treatment with Cur and EGCG. In control, higher red fluorescence intensity was seen due to the accumulation of JC-1 dye by the healthy mitochondria in the cells, indicating that the cells are alive and healthy. However, less accumulation of JC-1 dye was observed in the treated sample, indicating that the cells are apoptotic, as seen through an increase in green fluorescence. The ratio of red and green fluorescence intensity was quantified using ImageJ and plotted against all compositions, as shown in Fig. 4D, which shows a higher number of unhealthy cells in treatment. Fig. 4E shows the healthy fibroblast morphology of osteosarcoma cells in control and a highly ruptured and broken morphology of osteosarcoma cells for all treatments at day 3 and 11, supporting *in vitro* chemopreventive potential of Cur and EGCG.

3.4. Cur and EGCG promote osteoblast proliferation and differentiation

To evaluate the effect of Cur and EGCG on osteoblast proliferation and differentiation, *in vitro* osteoblast study was performed for 3, 7, and 11 days. Fig. 5A shows that cell viability increases in both control and treated samples, verifying their non-toxic behavior toward healthy osteoblast cells. Compared to the control, an increase in cell viability was observed for Cur, EGCG, and the combined EGCG and Cur system. At day 11, Cur and EGCG showed a 1.8-fold and 2-fold increase in osteoblast growth compared to the control. The combined dual drug system results in a 3-fold increase in cellular viability compared to the untreated sample. It was found that the combined system showed a 1.7-fold and 1.5-fold increase in cellular viability as compared to Cur and EGCG, respectively, suggesting its synergistic effect in promoting osteoblast proliferation ($p < 0.01$). Live/dead imaging shown in Fig. 5B reveals only live cells on all samples, as seen through green fluorescence intensity, supporting the cytocompatibility of the treated sample toward osteoblast cells.

Fig. 5C shows ALP assay results where Cur and EGCG showed higher absorbance, indicating enhanced differentiation activity compared to the control. This was also validated using ALP staining where higher green fluorescence, indicating ALP marker was observed in Cur and EGCG treated samples, as shown in Fig. 5D. Surface morphology demonstrated in Fig. 5E shows osteoblast cell morphology after different time points. On day 3, filopodia extensions were seen in all samples. At 11 days, matured cell morphology and attachment were observed all over the surface, supporting the cytocompatibility and osteoblast proliferation ability of Cur and EGCG-treated implants.

3.5. Antibacterial activity of Cur and EGCG against S. aureus

The current work assesses the antibacterial efficacy of both EGCG and Cur against *S. aureus*. Fig. 6A shows images of agar plates with a colony of bacteria growing on them. For the Cur and EGCG-treated samples, less colony formation was observed than the control, indicating less viable bacterial colonies left after treatment with drugs, after 36 and 72 h. As shown in Fig. 6B, after 72 h, Cur exhibits ~58 % antibacterial efficacy, while EGCG shows ~65 % efficacy. However, the dual drug system shows an increase to ~94 % efficacy. This is also validated using live/dead imaging, where high green fluorescence was seen in control, indicating live bacteria.

In contrast, increased red fluorescence was observed in the treated samples, indicating dead bacteria. The plot from the live/dead imaging also shows a decrease in the bacterial cell viability in the treated samples, as shown in Fig. 6D, which aligns with the results of the agar plates. Fig. 6E shows the morphology of only HA and drug-loaded samples. In untreated samples, dense bacterial colonies were observed, while in the case of Cur and EGCG-loaded samples, fewer colonies were observed, supporting their ability to inhibit the growth of bacteria.

4. Discussion

Several bone-related diseases, such as tumor ablation, osteoporosis, and osteomyelitis at times, result in critical size bone defects that do not self-repair. Osteosarcoma tumor

resection surgery also does not completely eradicate the cancer cells, creating a bone defect and increasing the chances of bone metastasis. The current work tries to address these challenges by developing a novel multifunctional implant loaded with natural medicinal compounds. The results indicate that controlled and sustained release of both Cur and EGCG from HA-coated titanium inhibits the growth of osteosarcoma cells, promotes bone formation *in vitro,* and shows antibacterial properties against *S. aureus*.

The controlled delivery of chemotherapeutic drugs to the desired site without causing cytotoxicity to normal cells is a common challenge in cancer treatment. Localized delivery of these drugs not only helps in reducing side effects to healthy tissues but also improves their overall therapeutic efficacy. [49] In addition to having osteoconductive behavior, calcium phosphates can also adsorb a drug physically and chemically and deliver it to the target in a controlled manner. [50] This makes them a suitable drug carrier to deliver therapeutics to treat different diseases.

Post-tumor resection surgery, the pH of the microenvironment around the defect site becomes acidic. The release study carried out at pH 5.0 shows that both drugs exhibit initial burst release followed by sustained release. Due to the high solubility of EGCG in buffer solutions, it releases faster and more, reaching 32 % in 24 h, while Cur, which has less solubility in water, releases slower. The initial burst release of these drugs through the coated implant would assist in avoiding immediate post-operative surgery inflammation, infection and inhibit tumor growth. This would be followed by sustained release of Cur when pH gets back to 7.4 after two weeks, which would eradicate any remaining tumor cells, promote wound healing, and promote osteogenesis for the desired period. [51] The dissolution properties of the HA coating in the media also depend on the pH of the surrounding environment. The implants kept at low pH show higher coating dissolution and leaching, as shown in Fig. 3, while at pH 7.4, the coating over the implant stays intact. At pH 5.0, higher coating degradation led to a higher release % of Cur when compared to release % at pH 7.4, while in the case of EGCG, the pKa-pH factor dominated, and overall higher release was seen at pH 7.4 than at pH 5.0. The cumulative release profiles were also fit using power law and the weibull model to predict future release behavior.

After evaluating the release behavior of Cur and EGCG, an *in vitro* osteosarcoma study was carried out next to assess the anti-cancer efficacy of the drugs. From the study, it was found that both Cur and EGCG exhibit anti-cancer properties against osteosarcoma cells. <70 % osteosarcoma cellular viability was observed for all the treated samples after 7 and 11 days, which indicates their cytotoxic potential as per ISO-10993–1 standard. [52] Both EGCG and Cur are known to modulate multiple cell signaling pathways, including the downregulation of the NF- κB pathway. [53] As shown in Fig. 7, in the normal state, the inactive NF-κB rest in the cell in conjugation with IκB. However, phosphorylation of this conjugate by external or internal stimuli causes it to dissociate from IκB and become active. This NF- κB in the activated state then translocates to the nuclei, binds to the cell DNA, and causes tumor cell proliferation. Cur and EGCG are known to inhibit phosphorylation, which causes NF-κB to stay in the inactive state and inhibit tumor proliferation.

Next, the effect of EGCG and Cur on the cell viability of osteoblast, a bone-forming cell, was studied. The results indicate that both EGCG and Cur show cytocompatibility toward osteoblast cells. All samples showed excellent cellular attachment on the surface. MTT and ALP results indicate that Cur and EGCG promote the proliferation and maturation of healthy osteoblast cells. One of our previous studies has also reported the positive effect of Cur on *in vivo* osseointegration ability using *in vivo* rat distal femur model [9] It has been reported that Cur enhances the osteocalcin and Runx2 expression, which leads to osteoblast cell proliferation and differentiation. The positive effect of EGCG on osteoblast proliferation also aligns with a recent study that reported similar results. [27] EGCG promotes osteoblast maturation by upregulating the Runx2 and BGLAP genes, osteoblast-specific target genes. [27] Runx 2 is expressed in the early stage of osteoblast differentiation, while BGLAP is expressed in the later stage of differentiation, which causes bone mineralization. [54] Both genes are regulated by EGCG *via* the wnt/B-catenin signaling pathway. [55] The sustained release of Cur and EGCG would accelerate osteoblast proliferation and maturation at the defect site, helping in faster bone healing.

Even after the successful implantation of an HA-coated metallic implant at the site, many post-implantation concerns arise, leading to implant removal or revision surgery. One of the major concerns is bacterial infection. Our results show that both Cur and EGCG inhibit the growth of *S. aureus.* After 72 h, with maximum antibacterial efficacy observed in the combined EGCG and Cur system. Many studies have reported that Cur ruptures the permeability and membrane integrity of bacterial cell membranes by creating reactive oxygen species, leading to bacterial cell death. [56] Curcumin is also found to bind to Filamenting temperature-sensitive mutant Z (FtsZ) proteins, a protein that helps in cell division. This binding step inhibits the assembly of FtsZ with protofilaments, which in turn inhibits the cell division of bacteria. [57] EGCG is another well-researched antibacterial agent known to damage the bactericidal film, which enhances the penetration of EGCG into the interior of the bacteria and causes bacteria to rupture. [58] It has also been reported that EGCG can bind to the membrane of the bacteria and can interfere with the lipid bilayer, proteins, or peptide *via* hydrogen bonding. [59]

After evaluating all the studies performed on this system, it could be summarized that an HA-coated Ti64 implant incorporated with Cur and EGCG could be used as a potential multi-functional bone graft to enhance *in vitro* chemoprevention and osteogenic potential. It could assist in treating bone tumors, promote osteoblast proliferation and differentiation, and prevent bone infection by acting as a localized and sustained drug delivery system.

5. Conclusion

This study shows that the controlled release of Cur and EGCG from HA-coated titanium exhibits *in vitro* chemopreventive potential, cytocompatibility toward osteoblast cells, and anti-bacterial efficacy against *S. aureus*. An *In vitro* release study conducted at acidic and physiological mediums reveals a controlled and sustained release profile of Cur and EGCG from HA-coated implants. Both Cur and EGCG exhibit cytotoxicity toward human osteosarcoma cells, indicating *in vitro* chemopreventive ability. *In vitro* osteoblast studies demonstrate that both NMCs show cytocompatibility with bone-forming cells and further

enhance their proliferation and differentiation, suggesting *in vitro* osteogenic potential. The results also indicate the antibacterial efficacy of Cur and EGCG against *S. aureus*, a primary cause of infection in orthopedic implants. Although further *in vivo* work can provide an in-depth understanding of both anti-tumor properties and osteogenesis, this work serves as a building block to develop multifunctional load-bearing implants for orthopedic and dental applications.

Acknowledgments

The authors acknowledge financial support from the National Institute of Arthritis and Musculoskeletal and Skin Diseases (NIAMS) of the National Institutes of Health (NIH) under grant number R01 AR066361–06 (PI: Bose) and the National Institute of Dental and Craniofacial Research (NIDCR) of NIH under grant number R56 DE029204 – 01(PI: Bose). The authors also acknowledge the Franceschi Microscopy and Imaging Center at Washington State University.

Data availability

Data will be made available on request.

References

[1]. Martin V, Bettencourt A, Bone regeneration: biomaterials as local delivery systems with improved osteoinductive properties, Mater. Sci. Eng. C 82 (2018) 363–371, 10.1016/j.msec.2017.04.038.

[2]. Herberg S, McDermott AM, Dang PN, Alt DS, Tang R, Dawahare JH, Varghai D, Shin J-Y, McMillan A, Dikina AD, He F, Lee YB, Cheng Y, Umemori K, Wong PC, Park H, Boerckel JD, Alsberg E, Combinatorial morphogenetic and mechanical cues to mimic bone development for defect repair, Sci. Adv. 5 (2019), eaax2476, 10.1126/sciadv.aax2476. [PubMed: 31489377]

[3]. Kravanja KA, Finšgar M, A review of techniques for the application of bioactive coatings on metal-based implants to achieve controlled release of active ingredients, Mater. Des. 217 (2022), 110653.

[4]. Wu Z, Chan B, Low J, Chu JJH, Hey HWD, Tay A, Microbial resistance to nanotechnologies: an important but understudied consideration using antimicrobial nanotechnologies in orthopaedic implants, Bioact. Mater. 16 (2022) 249–270, 10.1016/j.bioactmat.2022.02.014. [PubMed: 35415290]

[5]. Meltzer PS, Helman LJ, New horizons in the treatment of osteosarcoma, N. Engl. J. Med. 385 (2021) 2066–2076. [PubMed: 34818481]

[6]. Mirabello L, Troisi RJ, Savage SA, Osteosarcoma incidence and survival rates from 1973 to 2004: data from the surveillance, epidemiology, and end results program, Cancer 115 (2009) 1531–1543. [PubMed: 19197972]

[7]. Tian H, Cao J, Li B, Nice EC, Mao H, Zhang Y, Huang C, Managing the immune microenvironment of osteosarcoma: the outlook for osteosarcoma treatment, Bone Res. 11 (2023) 11, 10.1038/s41413-023-00246-z. [PubMed: 36849442]

[8]. Bhattacharjee A, Bose S, Multifunctional polydopamine – Zn2+-curcumin coated additively manufactured ceramic bone grafts with enhanced biological properties, Biomater. Adv. 213487 (2023), 10.1016/j.bioadv.2023.213487. [PubMed: 37400297]

[9]. Sarkar N, Bose S, Controlled delivery of curcumin and vitamin K2 from hydroxyapatite-coated titanium implant for enhanced in vitro chemoprevention, osteogenesis, and in vivo osseointegration, ACS Appl. Mater. Interfaces 12 (2020) 13644–13656. [PubMed: 32013377]

[10]. Tobeiha M, Rajabi A, Raisi A, Mohajeri M, Yazdi SM, Davoodvandi A, Aslanbeigi F, Vaziri M, Hamblin MR, Mirzaei H, Potential of natural products in osteosarcoma treatment: focus on molecular mechanisms, Biomed. Pharmacother. 144 (2021), 112257, 10.1016/j.biopha.2021.112257. [PubMed: 34688081]

[11]. Alvi SB, Appidi T, Deepak BP, Rajalakshmi PS, Minhas G, Singh SP, Begum A, Bantal V, Srivastava R, Khan N, Rengan AK, The “nano to micro” transition of hydrophobic curcumin crystals leading to in situ adjuvant depots for Au-liposome nanoparticle mediated enhanced photothermal therapy, Biomater. Sci. 7 (2019) 3866–3875, 10.1039/C9BM00932A. [PubMed: 31309204]

[12]. Sadeghian M, Rahmani S, Jamialahmadi T, Johnston TP, Sahebkar A, The effect of oral curcumin supplementation on health-related quality of life: a systematic review and meta-analysis of randomized controlled trials, J. Affect. Disord. 278 (2021) 627–636. [PubMed: 33038707]

[13]. De Freitas CF, Kimura E, Rubira AF, Muniz EC, Curcumin and silver nanoparticles carried out from polysaccharide-based hydrogels improved the photodynamic properties of curcumin through metal-enhanced singlet oxygen effect, Mater. Sci. Eng. C 112 (2020), 110853, 10.1016/j.msec.2020.110853.

[14]. Khorasani MY, Langari H, Sany SBT, Rezayi M, Sahebkar A, The role of curcumin and its derivatives in sensory applications, Mater. Sci. Eng. C 103 (2019), 109792, 10.1016/j.msec.2019.109792.

[15]. Balaji S, Chempakam B, Toxicity prediction of compounds from turmeric (Curcuma longa L), Food Chem. Toxicol. 48 (2010) 2951–2959, 10.1016/j.fct.2010.07.032. [PubMed: 20667459]

[16]. Hsieh C, Phase I clinical trial of curcumin, a chemopreventive agent, in patients with high-risk or pre-malignant lesions, Anticancer Res. 21 (2001), e2900.

[17]. Sharma RA, Euden SA, Platton SL, Cooke DN, Shafayat A, Hewitt HR, Marczylo TH, Morgan B, Hemingway D, Plummer SM, Phase I clinical trial of oral curcumin: biomarkers of systemic activity and compliance, Clin. Cancer Res. 10 (2004) 6847–6854. [PubMed: 15501961]

[18]. Hatcher H, Planalp R, Cho J, Torti F, Torti S, Curcumin: from ancient medicine to current clinical trials, Cell. Mol. Life Sci. 65 (2008) 1631–1652. [PubMed: 18324353]

[19]. Chang R, Chen L, Qamar M, Wen Y, Li L, Zhang J, Li X, Assadpour E, Esatbeyoglu T, Kharazmi MS, Li Y, Jafari SM, The bioavailability, metabolism and microbial modulation of curcumin-loaded nanodelivery systems, Adv. Colloid Interf. Sci. 318 (2023), 102933, 10.1016/j.cis.2023.102933.

[20]. Mokhtari RB, Homayouni TS, Baluch N, Morgatskaya E, Kumar S, Das B, Yeger H, Combination therapy in combating cancer, Oncotarget 8 (2017) 38022–38043, 10.18632/oncotarget.16723. [PubMed: 28410237]

[21]. Jin G, Yang Y, Liu K, Zhao J, Chen X, Liu H, Bai R, Li X, Jiang Y, Zhang X, Lu J, Dong Z, Combination curcumin and (−)-epigallocatechin-3-gallate inhibits colorectal carcinoma microenvironment-induced angiogenesis by JAK/STAT3/IL-8 pathway, Oncogenesis 6 (2017), 10.1038/oncsis.2017.84 e384–e384. [PubMed: 28967875]

[22]. Chu C, Wang Y, Wang Y, Yang R, Liu L, Rung S, Xiang L, Wu Y, Du S, Man Y, Qu Y, Evaluation of epigallocatechin-3-gallate (EGCG) modified collagen in guided bone regeneration (GBR) surgery and modulation of macrophage phenotype, Mater. Sci. Eng. C 99 (2019) 73–82, 10.1016/j.msec.2019.01.083.

[23]. Leone M, Zhai D, Sareth S, Kitada S, Reed JC, Pellecchia M, Cancer prevention by tea polyphenols is linked to their direct inhibition of antiapoptotic Bcl-2-family proteins, Cancer Res. 63 (2003) 8118–8121. [PubMed: 14678963]

[24]. Chen B-H, Hsieh C-H, Tsai S-Y, Wang C-Y, Wang C-C, Anticancer effects of epigallocatechin-3-gallate nanoemulsion on lung cancer cells through the activation of AMP-activated protein kinase signaling pathway, Sci. Rep. 10 (2020) 5163, 10.1038/s41598-020-62136-2. [PubMed: 32198390]

[25]. Yang G-Y, Effect of black and green tea polyphenols on c-jun phosphorylation and H2O2 production in transformed and non-transformed human bronchial cell lines: possible mechanisms of cell growth inhibition and apoptosis induction, Carcinogenesis 21 (2000) 2035–2039, 10.1093/carcin/21.11.2035. [PubMed: 11062165]

[26]. Tokuda H, Takai S, Matsushima-Nishiwaki R, Akamatsu S, Hanai Y, Hosoi T, Harada A, Ohta T, Kozawa O, (−)-epigallocatechin gallate enhances prostaglandin F2α-induced VEGF synthesis via upregulating SAPK/JNK activation in osteoblasts, J. Cell. Biochem. 100 (2007) 1146–1153. [PubMed: 17031857]

[27]. Jo Y, Sarkar N, Bose S, In vitro biological evaluation of epigallocatechin gallate (EGCG) release from three-dimensional printed (3DP) calcium phosphate bone scaffolds, J. Mater. Chem. 11 (2023) 5503–5513.

[30]. Vahabzadeh S, Roy M, Bandyopadhyay A, Bose S, Phase stability and biological property evaluation of plasma sprayed hydroxyapatite coatings for orthopedic and dental applications, Acta Biomater. 17 (2015) 47–55, 10.1016/j.actbio.2015.01.022. [PubMed: 25638672]

[31]. Wang B, Li Y, Wang S, Jia F, Bian A, Wang K, Xie L, Yan K, Qiao H, Lin H, Lan J, Huang Y, Electrodeposited dopamine/strontium-doped hydroxyapatite composite coating on pure zinc for anti-corrosion, antimicrobial and osteogenesis, Mater. Sci. Eng. C 129 (2021), 112387, 10.1016/j.msec.2021.112387.

[34]. Bose S, Sarkar N, Vahabzadeh S, Sustained release of vitamin C from PCL coated TCP induces proliferation and differentiation of osteoblast cells and suppresses osteosarcoma cell growth, Mater. Sci. Eng. C 105 (2019), 110096, 10.1016/j.msec.2019.110096.

[35]. Nayak C, Kushram P, Zaidi MAA, Singh I, Sen J, Balani K, Multi-length scale strengthening and cytocompatibility of ultra high molecular weight polyethylene bio-composites by functionalized carbon nanotube and hydroxyapatite reinforcement, J. Mech. Behav. Biomed. Mater. 140 (2023), 105694, 10.1016/j.jmbbm.2023.105694. [PubMed: 36841125]

[36]. Ambre A, Katti KS, Katti DR, In situ mineralized hydroxyapatite on amino acid modified nanoclays as novel bone biomaterials, Mater. Sci. Eng. C 31 (2011) 1017–1029, 10.1016/j.msec.2011.03.001.

[37]. Yazici H, Habib G, Boone K, Urgen M, Utku FS, Tamerler C, Self-assembling antimicrobial peptides on nanotubular titanium surfaces coated with calcium phosphate for local therapy, Mater. Sci. Eng. C 94 (2019) 333–343, 10.1016/j.msec.2018.09.030.

[38]. Campoccia D, Montanaro L, Arciola CR, The significance of infection related to orthopedic devices and issues of antibiotic resistance, Biomaterials 27 (2006) 2331–2339. [PubMed: 16364434]

[39]. Bhawana RK, Basniwal HS, Buttar VK, Jain N, Jain, Curcumin nanoparticles: preparation, characterization, and antimicrobial study, J. Agric. Food Chem. 59 (2011) 2056–2061, 10.1021/jf104402t. [PubMed: 21322563]

[40]. Zhao W-H, Hu Z-Q, Okubo S, Hara Y, Shimamura T, Mechanism of synergy between Epigallocatechin Gallate and β-Lactams against methicillin-resistant *Staphylococcus aureus*, Antimicrob. Agents Chemother. 45 (2001) 1737–1742, 10.1128/AAC.45.6.1737-1742.2001. [PubMed: 11353619]

[41]. Vu AA, Bose S, Natural antibiotic oregano in hydroxyapatite-coated titanium reduces osteoclastic bone resorption for orthopedic and dental applications, ACS Appl. Mater. Interfaces 12 (2020) 52383–52392, 10.1021/acsami.0c14993. [PubMed: 33181015]

[42]. A. Designation, C33, Standard Specification for Concrete Aggregates, July, ASTM International, USA, 2003, p. 8.

[43]. Jørgensen K, Jacobsen L, Factorial design used for ruggedness testing of flow through cell dissolution method by means of Weibull transformed drug release profiles, Int. J. Pharm. 88 (1992) 23–29, 10.1016/0378-5173(92)90300-Q.

[44]. Bruschi ML, Strategies to Modify the Drug Release from Pharmaceutical Systems, Woodhead Publishing, 2015.

[45]. Fielding GA, Roy M, Bandyopadhyay A, Bose S, Antibacterial and biological characteristics of silver containing and strontium doped plasma sprayed hydroxyapatite coatings, Acta Biomater. 8 (2012) 3144–3152, 10.1016/j.actbio.2012.04.004. [PubMed: 22487928]

[46]. Wang L, Wang M, Li M, Shen Z, Wang Y, Shao Y, Zhu Y, Trace fluorine substituted calcium deficient hydroxyapatite with excellent osteoblastic activity and antibacterial ability, CrystEngComm 20 (2018) 5744–5753, 10.1039/C8CE01325J.

[47]. ISO—International Organization for Standardization, ISO 13779–2: 2018—Implants for Surgery—Hydroxyapatite—Part 2: Thermally Sprayed Coatings of Hydroxyapatite, 2018.

[48]. Muzolf M, Szymusiak H, Gliszczyńska-Świgło A, Rietjens IM, ena Tyrakowska B, pH-dependent radical scavenging capacity of green tea catechins, J. Agric. Food Chem. 56 (2008) 816–823. [PubMed: 18179168]

[49]. Aquib M, Juthi AZ, Farooq MA, Ali MG, Janabi AHW, Bavi S, Banerjee P, Bhosale R, Bavi R, Wang B, Advances in local and systemic drug delivery systems for post-surgical cancer treatment, J. Mater. Chem. B 8 (2020) 8507–8518, 10.1039/D0TB00987C. [PubMed: 32839803]

[50]. Bose S, Tarafder S, Calcium phosphate ceramic systems in growth factor and drug delivery for bone tissue engineering: a review, Acta Biomater. 8 (2012) 1401–1421, 10.1016/j.actbio.2011.11.017. [PubMed: 22127225]

[51]. Sarkar N, Bose S, Liposome-encapsulated curcumin-loaded 3D printed scaffold for bone tissue engineering, ACS Appl. Mater. Interfaces 11 (2019) 17184–17192. [PubMed: 30924639]

[52]. International Organization for Standardization (ISO 10993–5) 2009 Biological evaluation of medical devices—Part 5: tests for in vitro cytotoxicity., (n.d.).

[53]. Yang C, Zhu K, Yuan X, Zhang X, Qian Y, Cheng T, Curcumin has immunomodulatory effects on RANKL-stimulated osteoclastogenesis in vitro and titanium nanoparticle-induced bone loss in vivo, J. Cell. Mol. Med. 24 (2020) 1553–1567. [PubMed: 31845532]

[54]. Huang X, Guo X, Qu L, Wu Z, Yu T, Jiao Y, Zhou C, Gradient regulation of osteo-immune microenvironment by chitooligosaccharide-containing ion-doped mesoporous silica nanoparticles to accelerate osteogenesis, Appl. Mater. Today 23 (2021), 101067, 10.1016/j.apmt.2021.101067.

[55]. Wang J, Sun Q, Wei Y, Hao M, Tan W-S, Cai H, Sustained release of epigallocatechin-3-gallate from chitosan-based scaffolds to promote osteogenesis of mesenchymal stem cell, Int. J. Biol. Macromol. 176 (2021) 96–105, 10.1016/j.ijbiomac.2021.02.060. [PubMed: 33577812]

[56]. Varshney G, Saini R, Gupta P, Das K, Effect of curcumin on the diffusion kinetics of a hemicyanine dye, LDS-698, across a lipid bilayer probed by second harmonic spectroscopy, Langmuir 29 (2013) 2912–2918. [PubMed: 23391287]

[57]. Xiao J, Goley ED, Redefining the roles of the FtsZ-ring in bacterial cytokinesis, Curr. Opin. Microbiol. 34 (2016) 90–96, 10.1016/j.mib.2016.08.008. [PubMed: 27620716]

[58]. Ikigai H, Nakae T, Hara Y, Shimamura T, Bactericidal catechins damage the lipid bilayer, Biochim. Biophys. Acta BBA Biomembr. 1147 (1993) 132–136.

[59]. Yoda Y, Hu Z-Q, Shimamura T, Zhao W-H, Different susceptibilities of Staphylococcus and Gram-negative rods to epigallocatechin gallate, J. Infect. Chemother. 10 (2004) 55–58, 10.1007/s10156-003-0284-0. [PubMed: 14991521]

[60]. Balla VK, Xue W, Bose S, Bandyopadhyay A, Laser-assisted Zr/ZrO2 coating on Ti for load-bearing implants, Acta Biomaterialia 5 (2009) 2800–2809, 10.1016/j.actbio.2009.03.032. [PubMed: 19398221]

[61]. Roy M, Bandyopadhyay A, Bose S, Induction plasma sprayed nano hydroxyapatite coatings on titanium for orthopaedic and dental implants, Surf. Coat. Technol. 205 (2011) 2785–2792, 10.1016/j.surfcoat.2010.10.042. [PubMed: 21552358]

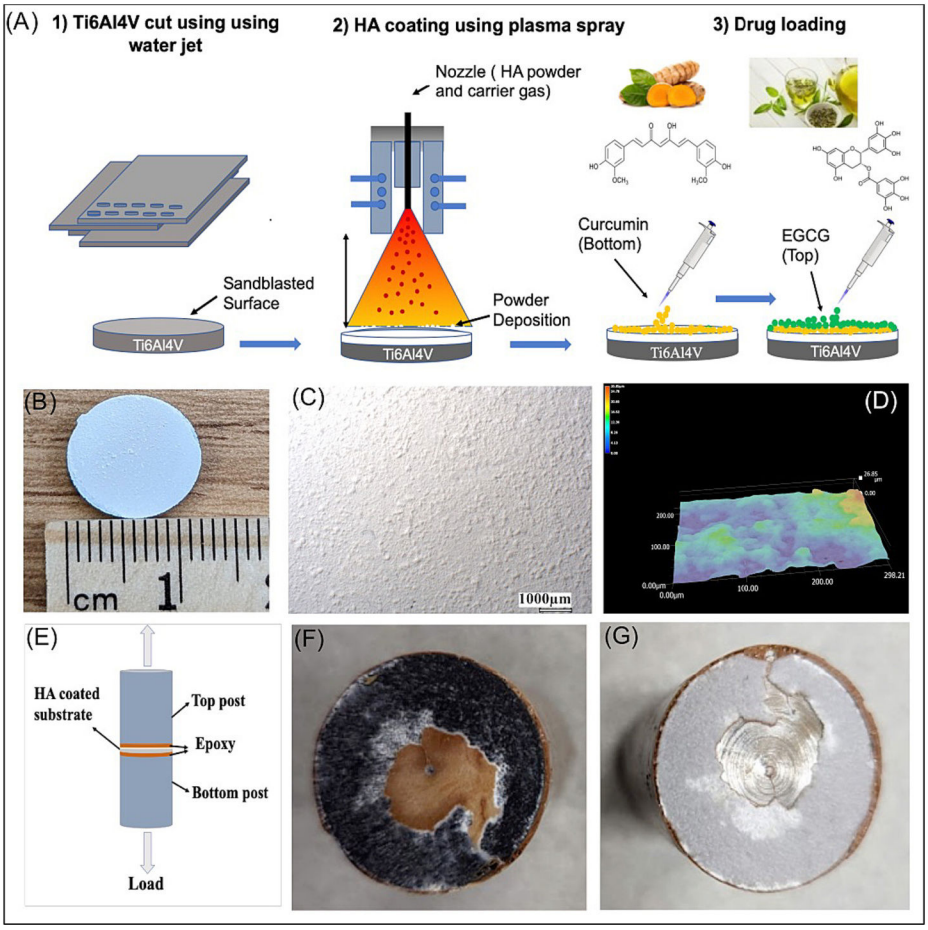

Fig. 1.

Schematic of the HA-coated implant preparation and mechanical characterization. (A) Step-by-step schematic of fabrication of Ti6Al4V implant coated with HA using plasma spray followed by drug loading using drop casting. (B) Image of the HA-coated implant after coating showing surface roughness. Images from stereomicroscope, (C) 2D image, and (D) 3D plot. (E) Schematic of tensile strength testing of HA coated implant shows load applied on both sides, testing adhesion strength between the implant and HA coating. Images of (F) the bottom post with adhered coating and (G) the top post with the rest of the HA coating adhered to the epoxy resin.

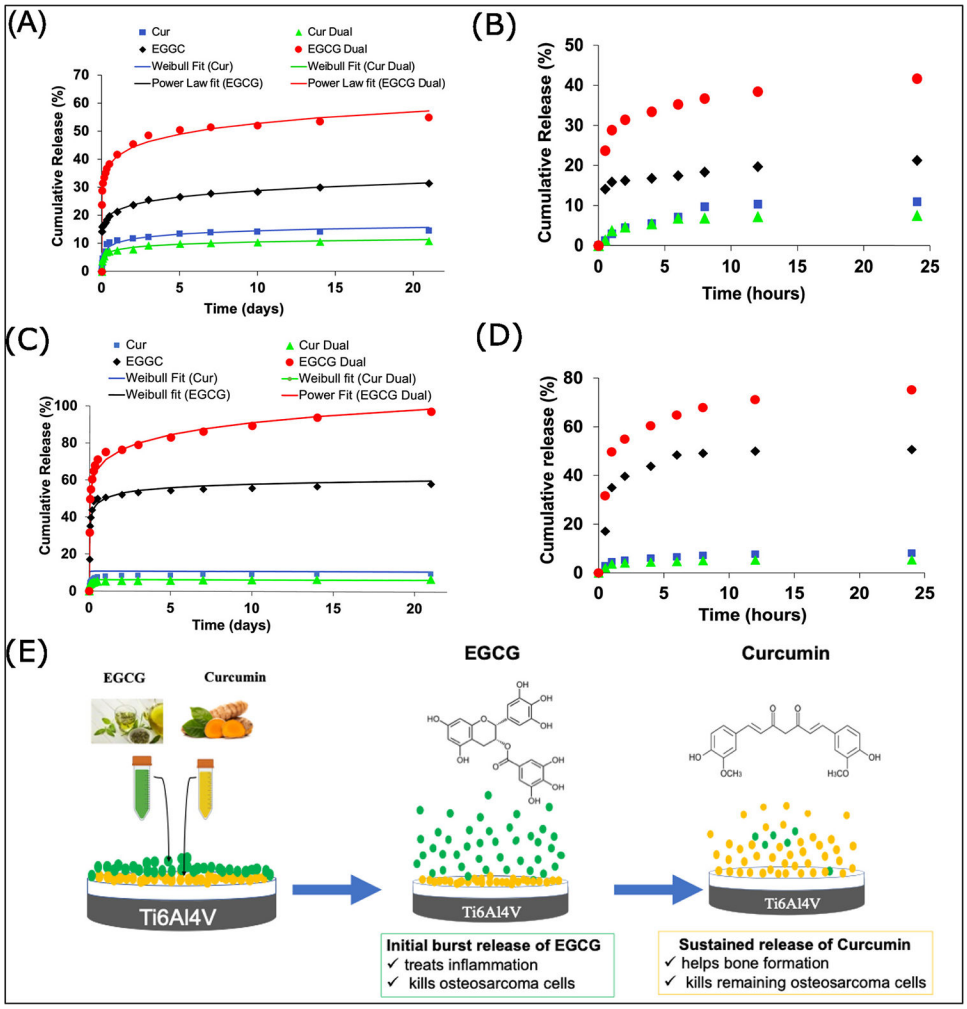

Fig. 2.

In vitro release profile of curcumin and EGCG from HA-coated titanium. (A) Release plot of individual curcumin and EGCG, and in the presence of each other at pH 5.0, all exhibiting biphasic controlled and sustained release profile. (B) Release plots of both drugs in the initial 24 h at pH 5.0. (C) Release plot of individual curcumin and EGCG, and in the presence of each other at pH 7.4, showing biphasic release profile. (D) Release plot of both drugs in the first 24 h at pH 7.4. (E) A schematic representing a sequence of phases of drug release from the implant, with initial burst release of EGCG, followed by sustained release of curcumin.

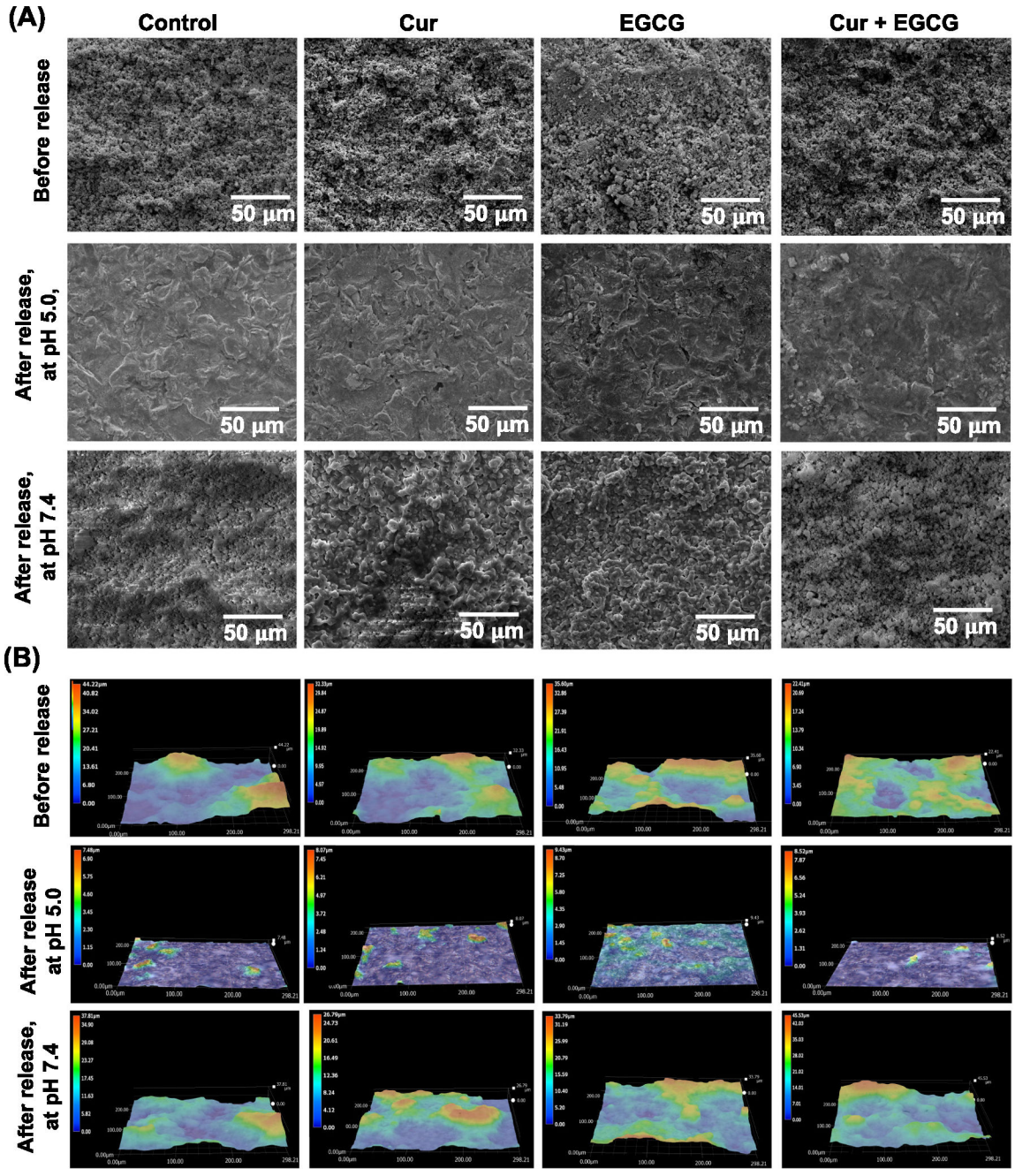

Fig. 3.

Surface morphology of drug-loaded implants after *in vitro* release study for 21 days. (A) FESEM images show higher coating dissolution and particle leaching at pH 5.0. compared to pH 7.4. (B) 3D mapping of implants taken using the stereomicroscope shows higher roughness of HA coating at pH 7.4 and before the release study; however, due to coating dissolution, low roughness or flat morphology of the implants was observed for all implants at pH 5.0.

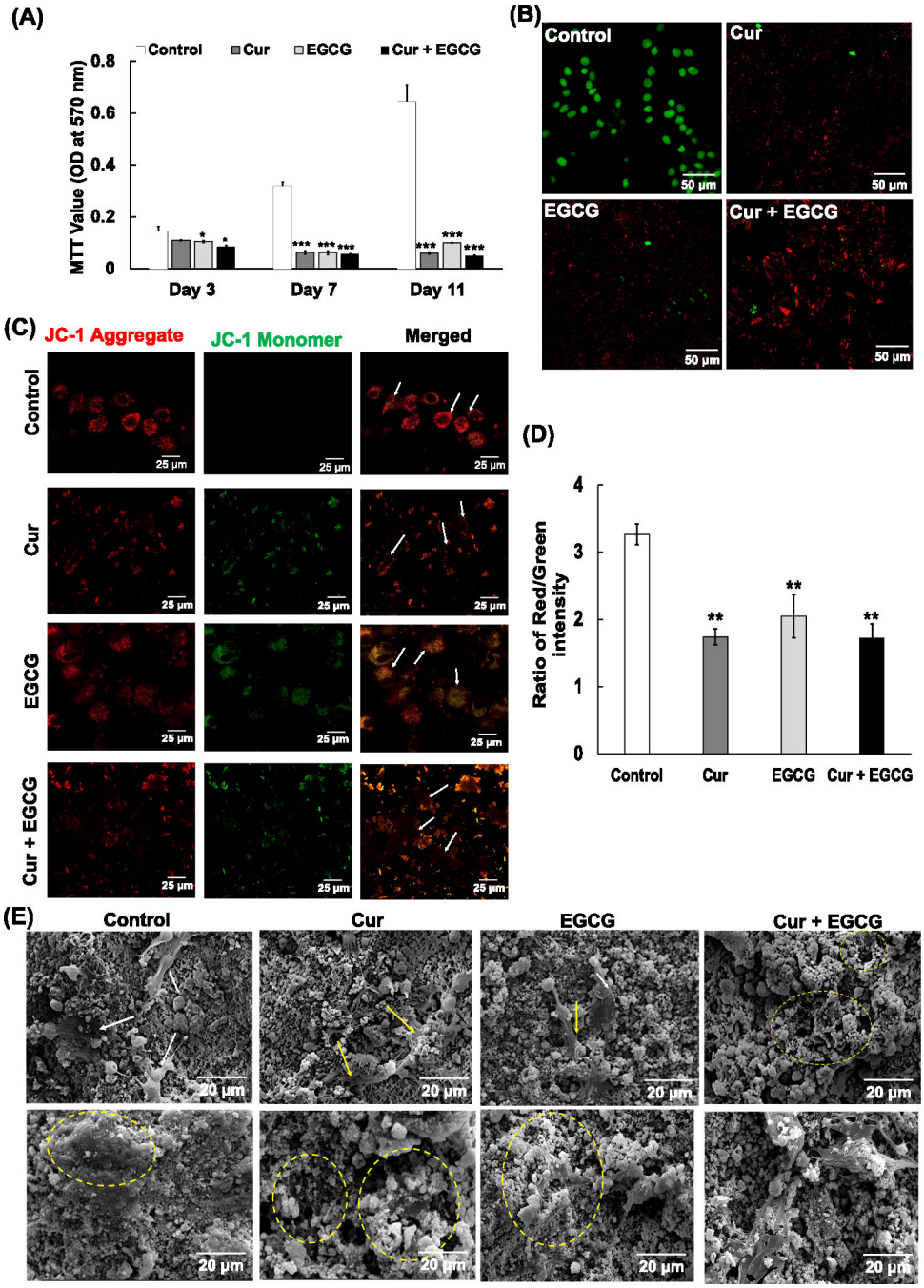

Fig. 4.

Results from *in vitro* osteosarcoma study performed with curcumin and EGCG dual drug system for 11 days. (A) MTT assay shows a reduction in the cell viability of osteosarcoma cells on treatment with curcumin and EGCG. (n = 3, * denotes $p \leq 0.05$, and ***denotes $p \leq 0.001$). (B) Live/dead imaging demonstrates live osteosarcoma cells in control (green fluorescence), while dead cells were observed in the treated implant (red fluorescence). (C) Mitochondrial membrane potential assay shows apoptosis in EGCG and curcumin-treated implants as shown through an increase in green fluorescence, indicating

low membrane potential of unhealthy mitochondria. Arrows marked in the images indicate the osteosarcoma cells. (D) Fluorescence intensity obtained through JC-1 assay quantified using ImageJ exhibits a decrease in the red/green fluorescence intensity ratio of the treated implant compared to the untreated sample. ($n = 3$, **denotes $p \leq 0.01$). (E) The surface morphology of osteosarcoma cells shows the ruptured morphology of osteosarcoma cells for all compositions, while the control exhibits healthy cellular attachment.

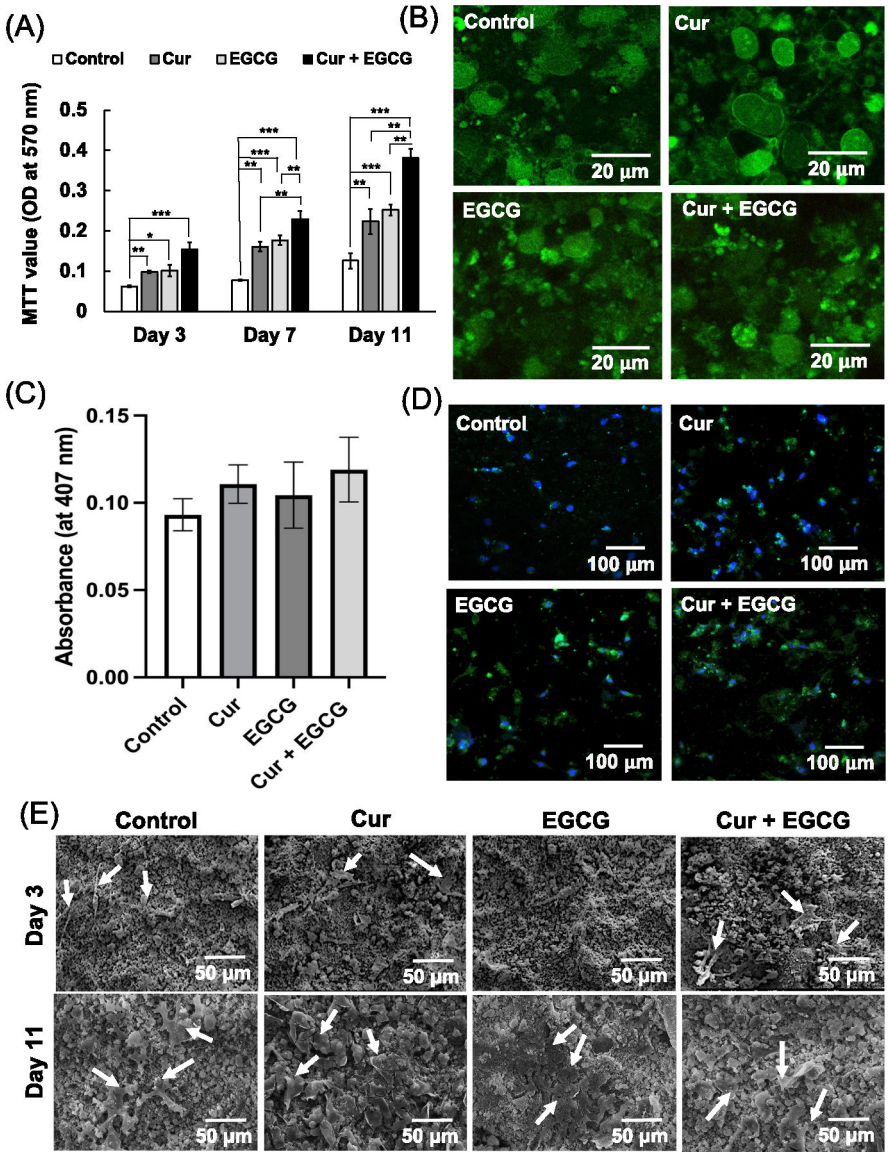

Fig. 5.

Results from *in vitro* osteoblast cell viability study against curcumin and EGCG dual drug delivery system for 11 days. (A) MTT assay illustrating the effect of control and different treatments on the osteoblast cellular viability. Both curcumin and EGCG enhance cellular viability compared to control, as shown through MTT assay (n = 3, * denotes $p \leq 0.05$, **denotes $p \leq 0.01$, and *** denotes $p \leq 0.001$). (B) Live/dead imaging performed using confocal laser microscopy reveals live cells in all samples (green fluorescence), supporting their cytocompatibility. The arrow marked in the images represents the osteoblast cells. (C) ALP assay shows that both drugs enhance the ALP differentiation activity compared to the control. (D) Higher ALP expression in drug-loaded implants was observed through higher green fluorescence. The blue dots indicate cell nuclei. (E) The surface morphology via FESEM exhibits healthy morphology and cellular attachment on both control and treated samples.

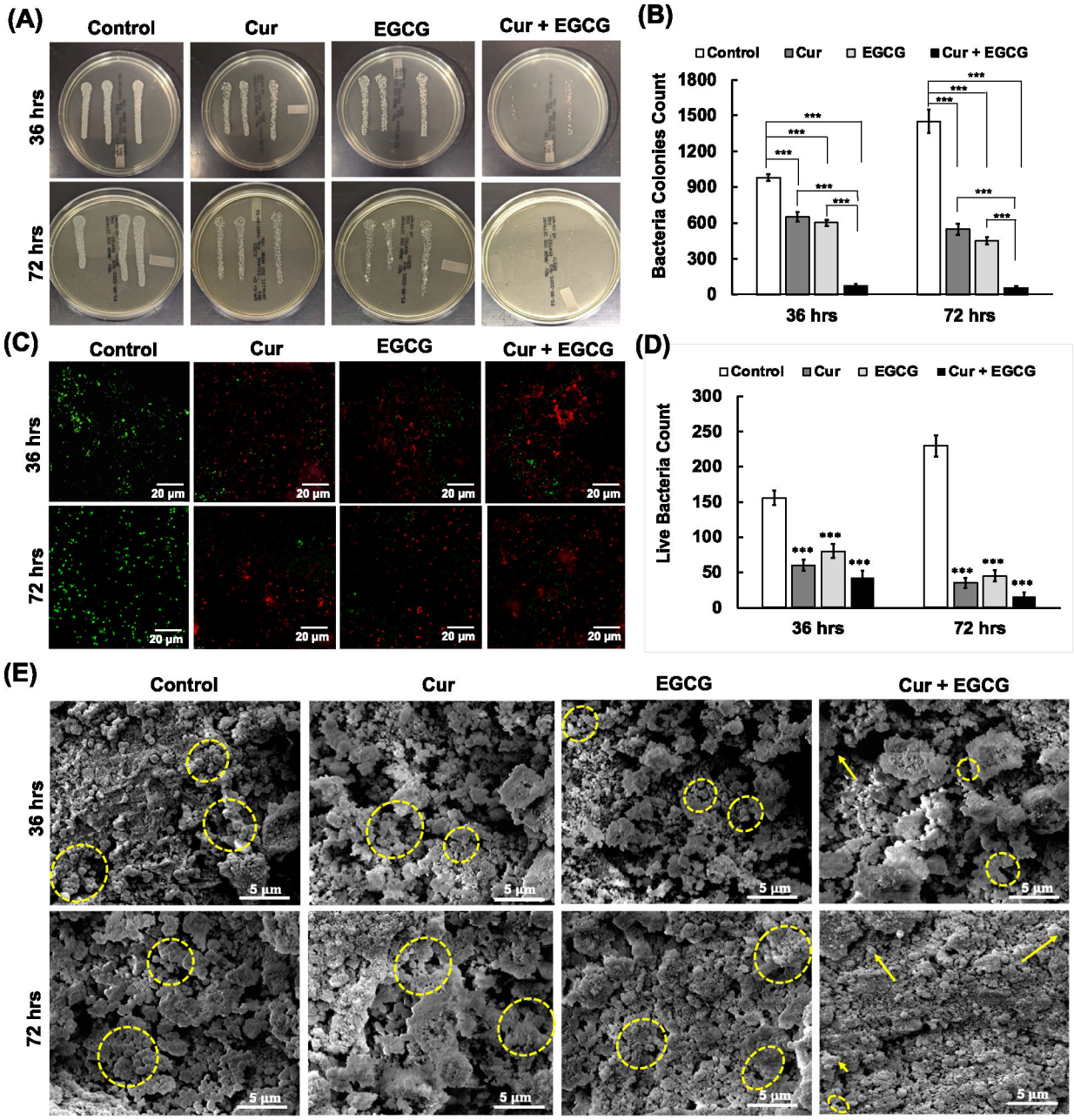

Fig. 6.

Results from the antibacterial study on dual drug system. (A) Agar plate images indicate a reduction in bacterial colony growth in the treated sample compared to the control, which showed dense colony formation. (B) The plot of bacterial colony counts after 36 and 72 h that the dual drug system enhances the antibacterial efficacy by 94 %. In contrast, curcumin showed an efficacy of ~ 58 %. EGCG showed ~ 65 % efficacy (n = 3, **denotes $p \leq 0.01$, and ***denotes $p \leq 0.001$) (C) Live/dead imaging shows higher green dots in control, indicating live bacteria. In comparison, higher red dots were observed in the treatment samples, indicating dead bacteria. (D) Quantification of the live/dead images shows a significantly reduced count of live bacteria in all the treated samples after 36 and

72 h (n = 3, ***denotes $p \leq 0.001$), supporting agar plate results. (E) Surface morphology through FESEM shows dense colonies in the untreated sample. In contrast, the treated sample showed fewer bacterial colonies.

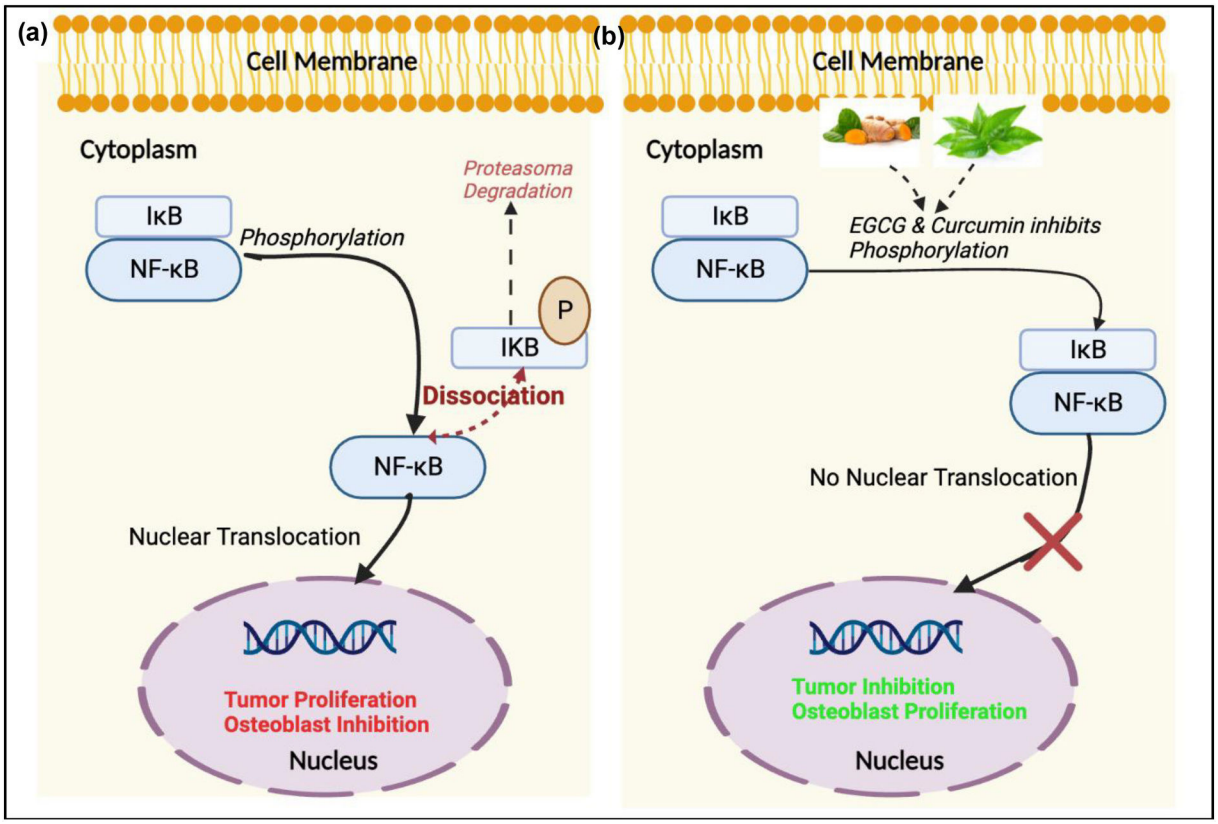

Fig. 7.

Proposed mechanism of action of curcumin and EGCG for tumor inhibition and bone osteoblast proliferation. (a) Activated IKKβ phosphorylates IκB, causes its subsequent degradation by enzyme proteasome, NF-κB heterodimer, translocates to the nucleus, and binds to the respective target genes in the DNA, promoting tumor growth and preventing osteoblast proliferation. (b) Both EGCG and curcumin suppress the phosphorylation of the IκB, avoiding the translocation to the nucleus to bind to their DNA elements, suppressing tumor growth, and promoting osteoblast proliferation.